Plasma plume characteristics and properties of pulsed laser deposited diamond-like carbon films

J. Haverkamp,[a] R. M. Mayo,[b] and M. A. Bourham
Department of Nuclear Engineering, North Carolina State University, Raleigh, North Carolina 27695-7909

J. Narayan and C. Jin
Department of Materials Science and Engineering, North Carolina State University, Raleigh, North Carolina 27695-7916

G. Duscher
Department of Materials Science and Engineering, North Carolina State University, Raleigh, North Carolina 27695-1916 and Solid State Division, Oak Ridge National Laboratory, Oak Ridge, Tennessee 37831-6030

(Received 14 August 2002; accepted 2 January 2003)

Pulsed laser deposition is a unique technique for the deposition of hydrogen-free diamond-like carbon films. During deposition, amorphous carbon is evaporated from a solid target by a high-energy KrF laser, ionized, and ejected as a plasma plume. The plume expands outwards and deposits the target material on a substrate. The plasma properties of the plume determine the quality of the thin films deposited on the substrate. These plume properties include ion density, ion flow speed, electron temperature, and plume peaking parameter. In this research, a triple Langmuir probe is used to determine various plasma properties of the plume created from the pulsed laser ablation of amorphous graphite as a function of laser energy density and laser spot size on the target. A thin diamond-like carbon film is deposited and analyzed with electron energy-loss spectroscopy to determine the sp^3/sp^2 fraction. A special preparation technique was used to prepare the thin film for analysis to prevent the damage that may be caused by conventional ion milling techniques. © *2003 American Institute of Physics.* [DOI: 10.1063/1.1555695]

I. INTRODUCTION

Diamond-like carbon (DLC) films have many properties similar to pure diamond including high hardness, scratch resistance, smooth surface morphology, chemical inertness, good thermal conductivity, high electrical resistance, and optical transparency.[1–3] These diamond-like properties make DLC films attractive for a number of applications including wear resistance in hip joints,[4] disk drive coatings,[5] flat panel displays,[1] and electron injection layers in organic light emitting diodes.[6] Diamond-like carbon films may be doped with certain elements to create and control unique tribological properties.[7]

Early work in diamond-like carbon films using chemical vapor deposition implied that hydrogen was necessary to preserve sp^3/sp^2 bonding in the films. The pulsed laser deposition (PLD) technique demonstrated that the presence of hydrogen is not necessary to obtain high quality DLC films.[2] Large sp^3/sp^2 bonding fractions, some higher than 80% have been reported in PLD films.[8] A review and discussion of preparation techniques for the production of DLC films is found in the previous literature.[1–3]

The details of the physical processes of target evaporation, plume creation and ionization, plume propagation, and the subsequent deposition of the DLC film itself are not known in detail and depend on a large number of operating variables. These variables include laser wavelength; laser spot size on the target; laser angle with respect to the target; laser pulse form; optical, mechanical and thermal properties of the target; substrate temperature; particle densities; ion kinetic energy; and forward peaking of the plume.[9–15] Recent work points to the kinetic energy of the ions as a key factor in the creation of high quality DLC thin films.[8,12,16] It was shown that an optimum ion kinetic energy exists near 90 eV.[8] However, similar work by Koivisaari finds an optimum ion kinetic energy of 450 eV.[12] One possible source of discrepancy is in the tendency to associate the Langmuir probe ion saturation time value data with a time-of-flight signal.

The interpretation of the Langmuir probe ion saturation current as a time-of-flight signal is not an obvious one. Collisions in the plume destroy the correspondence between arrival time and particle velocity distribution. Such collisions must occur during plume expansion, as they are a cause of the plume forward peaking, a phenomenon observed in the pulsed laser deposition process.[17] Additionally, a plume of finite initial dimension before expansion yields collisionless velocity space mixing. Furthermore, since the probe size is typically of the order of the plume dimensions, a correction for variation in ion density with respect to position must be applied.

In our work, flow speeds are calculated by examining leading edge arrival times at different probe positions. Flow speeds calculated by this method are nearly identical to those cited by Koivusaari,[12] although the laser energy densities in

[a]Electronic mail: jdhaverk@eos.ncsu.edu
[b]Present address: BLP, Inc., Cranbury, NJ 08518.

 © 2003 American Institute of Physics

Downloaded 11 Oct 2004 to 128.219.12.140. Redistribution subject to AIP license or copyright, see http://jap.aip.org/jap/copyright.jsp

that work were an order of magnitude higher than those in this work.

Understanding the role of plasma properties in the formation and quality of DLC films necessitates a detailed analysis of plasma and thin film properties as functions of the operating variables. The Langmuir probe is useful for the measurement of the properties of a variety of plasmas, including those within the plasma plume created in the PLD process.[18] This work presents a study of plasma properties determined by Langmuir probe analysis of the plasma plume created by the ablation of an amorphous carbon target by a KrF laser. Electron temperature, ion flow speed, ion kinetic energy, plume forward peaking parameter, and ion density are inferred from the Langmuir probe measurements. Laser energy density at the target and the spot size of the laser are varied independently. The Langmuir probe results are compared against an adiabatic expansion model.[19] Finally, the sp^3/sp^2 fraction of a thin DLC film, prepared with a special sample preparation technique that does not introduce damage to the film via ion milling,[20] is determined through electron energy-loss spectroscopy (EELS).

II. EXPERIMENT

The pulsed laser deposition system used for these experiments consists of an excimer laser, optical bench, a vacuum chamber, target holder, and various vacuum ports on the vacuum chamber. Details of the experimental system are described elsewhere.[9] The laser is a Lambda Physik KrF excimer laser capable of one-Joule laser pulses with a full pulse length of 45 ns and operates at a wavelength of 248 nm. The optical bench consists of several mirrors and lenses that direct the laser into the vacuum chamber at an angle of 45° to the target surface. Laser spot size on the target is independently controlled by fine positioning of the last focusing lens on the optical bench with respect to the vacuum chamber. The spots sizes on the target, estimated from burn patterns for this experiment were 0.22, 0.26, and 0.29 cm^2.

The target holder assembly forms the top of the vacuum chamber and permits the target to be rotated at approximately six resolutions per minute to prevent pitting. An amorphous carbon disk with a 1 in. diam supplied by Alfa Aesar is used as the target for both the Langmuir probe and deposition experiments. The graphite target was polished to prevent the occurrence of large particles within the plasma plume that have a deleterious effect on film quality.[21]

The Langmuir probe consists of three 5-mm-long tungsten tips connected to lead wire and fed through a vacuum tight Alumina tube. A Kepco power supply is used to bias the probe at -35 V such that one of the probe tips operates in ion saturation.[9] The Langmuir probe is inserted into the vacuum chamber through a Wilson seal that allows the probe to be moved toward and away from the target without breaking vacuum. The probe tips are placed 0.5 cm from the centerline of the laser spot. A Hewlett Packard 1153A differential probe connected to a Hewlett Packard Infinium oscilloscope is used to acquire voltage signals from a specially designed Langmuir probe circuit. The voltage signals are proportional to electron temperature and electron density.

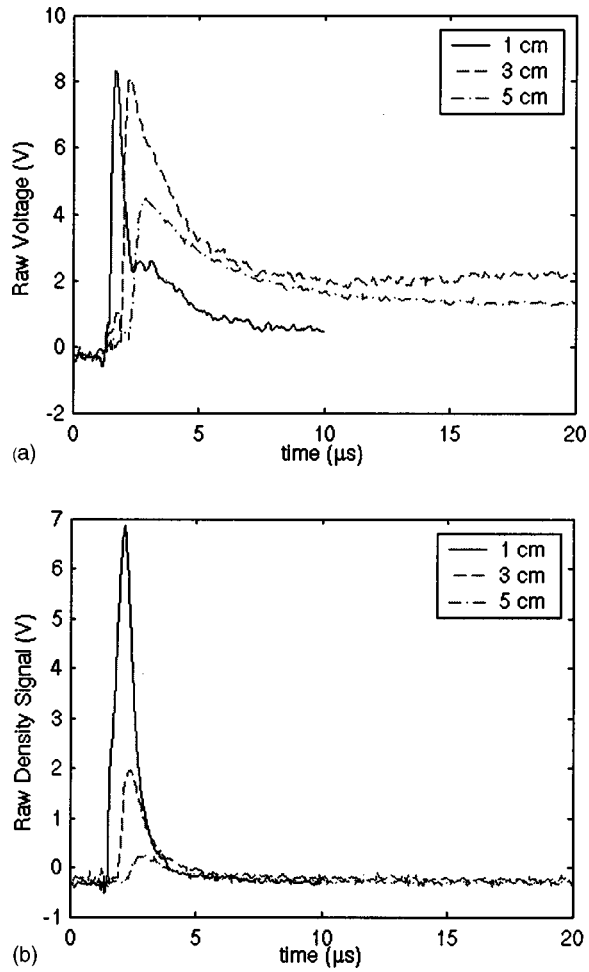

FIG. 1. (a) Raw voltage traces proportional to the electron temperature at Langmuir probe positions of 1, 3, and 5 cm. Laser energy 1000 mJ. Laser spot size on target 0.29 cm^2. (b) Raw voltage traces proportional to the ion density at Langmuir probe positions of 1, 3, and 5 cm. Laser energy 1000 mJ. Laser spot size on target 0.29 cm^2.

A Stanford Research Systems DG535 trigger generator is used to simultaneously trigger both the laser and data acquisition system. Density and temperature data were taken with the Langmuir probe at axial positions of 1, 3, and 5 cm from the target, laser spot sizes on target of 0.22, 0.26, and 0.29 cm^2; and laser energies from 350 to 1000 mJ in steps of 50 mJ. Example signals proportional to electron temperature and density are shown in Figs. 1(a) and 1(b).

Flow speeds at each laser energy and spot size are determined through the analysis of Langmuir probe signal arrival times. The raw density traces at the one and three centimeter Langmuir probe positions for identical laser energy and spot size conditions are normalized to the maximum value in each trace. The parallel components in the normalized raw density traces represent self-similar portions of the expanding plasma. The difference in the arrival times of the self-similar portions of the plasma at the one and three centimeter Langmuir probe positions is defined to be the drift time, Δt. Since the probe is not translated along the centerline of the plume, and since it cannot be assumed that the probe collects all particles at the tip of the probe, the plume travel distance between the 1 and 3 cm Langmuir probe positions is not

Downloaded 11 Oct 2004 to 128.219.12.140. Redistribution subject to AIP license or copyright, see http://jap.aip.org/jap/copyright.jsp

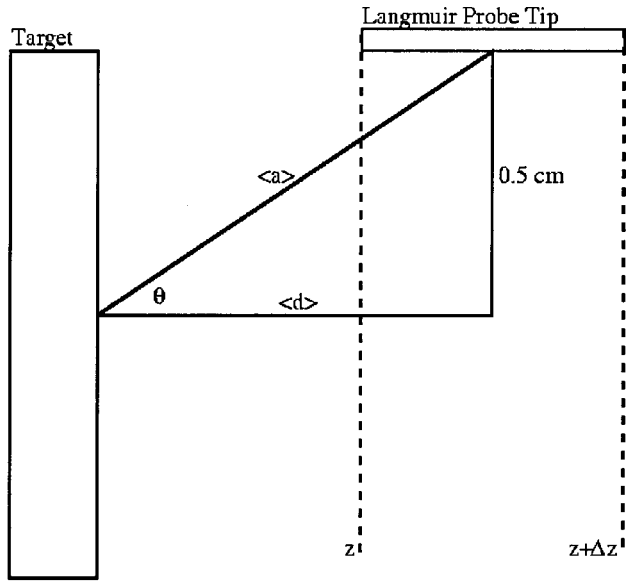

FIG. 2. Plasma collection geometry at Langmuir probe tip.

exactly 2 cm. A density-weighted average is used to calculate the axial position at which the probe may be considered to collect particles. If the density follows an inverse square relationship,[9] then the density averaged axial collecting distance, $\langle d \rangle$, is calculated using Eq. (1):

$$\langle d \rangle = \frac{\int_z^{z+\Delta z} \frac{1}{r^2} r\,dr}{\int_z^{z+\Delta z} \frac{1}{r^2}\,dr}. \tag{1}$$

As shown in Fig. 2, z and $z+\Delta z$ are the axial distances from the target surface. From the density averaged axial collecting distance, the average distance that the plasma travels to this collecting distance, $\langle a \rangle$, is calculated from:

$$\langle a \rangle = \frac{\langle d \rangle}{\cos\theta}. \tag{2}$$

The angle θ is calculated in terms of the offset of the probe from the centerline of the target as shown in Fig. 2:

$$\theta = \tan^{-1}\left(\frac{0.5\ \text{cm}}{\langle d \rangle}\right). \tag{3}$$

Given the drift time Δt, the distance traveled to the collection point at the 1 cm Langmuir probe position $\langle a_1 \rangle$ and the distance traveled to the collection point at the 3 cm Langmuir probe position $\langle a_3 \rangle$, the flow speed is calculated by

$$u = \frac{\langle a_3 \rangle - \langle a_1 \rangle}{\Delta t}. \tag{4}$$

The ion saturation current at the distance traveled to the collection point, $\langle a \rangle$, is the sum of those ions thermally crossing the sheath with the Bohm velocity and those collected as a result of the directed plume flow, the convective component. The local plume density, n_i, at the density averaged axial collection distance is calculated by

TABLE I. Important probe geometry values.

Z (cm)	θ (°)	$\langle d_j \rangle$ (cm)	$\langle a_j \rangle$ (cm)	$A_\perp$ (m^2)
1	22.3452	1.2164	1.3151	9.4×10^{-7}
3	8.7803	3.2372	3.2756	3.8×10^{-7}
5	5.4485	5.2421	5.2659	2.5×10^{-7}

$$n_i = \frac{i_{\text{sat}}}{0.61Ae\sqrt{\frac{kT_e}{M_i}} + A_\perp eu}, \tag{5}$$

where T_e is the electron temperature, M_i is the mass of the carbon ion, u the flow speed, and i_{sat} the ion saturation current recorded by the probe. The probe surface area A is 4×10^{-6} m^2. The second term in the denominator of Eq. (5) is a flow correction.[9] For supersonic flow, the area perpendicular to the flow $A_\perp$, the angle θ in Fig. 2, as well as values for $\langle a_j \rangle$ and $\langle d_j \rangle$ as a function of Langmuir probe position are included in Table I.

The plume ejected by pulsed laser ablation will not propagate isotropically, rather, it will be directed away from the target with forward peaking quantified via the parameter m in Eq. (6):[8]

$$n(r,\theta) = \frac{C}{r^2}\cos^m\theta. \tag{6}$$

Employing Eq. (6), data collected at three different Langmuir probe positions but constant laser energy and laser spot size is used to calculate m. Equation (5) is used to determine the peak density n at each Langmuir probe position j. When $\ln[(n_j/C)r_j^2]$ is plotted versus $\ln(\cos\theta_j)$ for the 1, 3, and 5 cm Langmuir probe positions, a straight line fit between these points will have a slope equal to the forward peaking factor m. Note that r_j is the average distance traveled to the collection point, $\langle a \rangle$, and that θ is the angle calculated by Eq. (3). The constant C is merely a scaling factor chosen to have a magnitude of the order of a typical plume density, for convenience of illustration. A sample $\ln[(n_j/C)r_j^2]$ vs $\ln(\cos\theta_j)$ graph is shown in Fig. 3.

Since the probe is displaced from the center of the spot by 0.5 cm, the ion density calculated at each Langmuir probe position is not the centerline plume density. To correct the signal at each Langmuir probe position j back to the centerline, Eq. (6) is employed so that

$$n(\langle d_j \rangle, 0) = \frac{n_j(\langle a_j \rangle, \theta_j)}{\cos^m\theta_j}. \tag{7}$$

Finally, a thin DLC film was deposited on a Si⟨100⟩ substrate of 100 μm thickness. The film was deposited by firing the laser with an energy density of 3.3 J/cm^2, with a spot size on target of 0.22 cm^2 for 55 s at 10 Hz. The thin (100 Å) DLC film is prepared for EELS through a chemical polishing technique. Small disks are cut and dimpled with an ultrasonic cutter from the deposited sample. Acid resistant wax is placed on the DLC coated side and the disk is placed

Downloaded 11 Oct 2004 to 128.219.12.140. Redistribution subject to AIP license or copyright, see http://jap.aip.org/jap/copyright.jsp

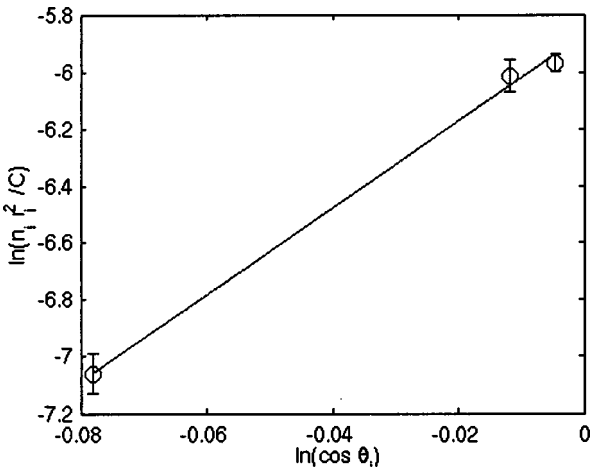

FIG. 3. Plot of $\ln[(n_j/C)r_j^2]$ vs $\ln(\cos\theta_j)$ for the sample case with laser energy of 1000 mJ, spot size on target of 0.26 cm^2 for the evaluation of *m*. *m* is 15.2097 ± 1.0324 in this case.

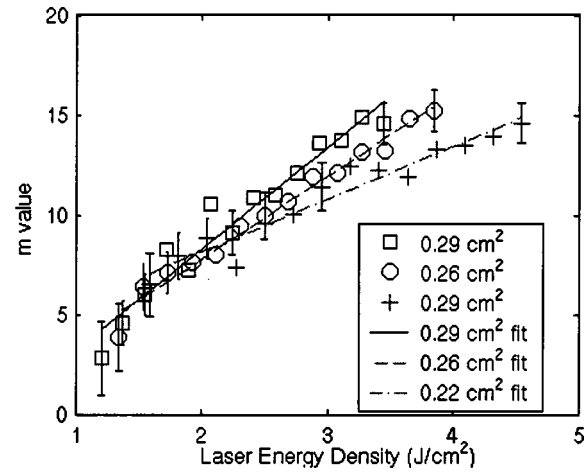

FIG. 4. Plume forward peaking parameters as a function of laser energy density and spot size. Linear fit lines to the data are drawn to show trends.

in an acid solution so that a small hole is created at the location of the dimple. When the wax is removed with solvents, the disk is then ready for EELS analysis. This chemical method has advantage over traditional ion milling methods by not introducing ion bombardment damage that can reduce the sp^3/sp^2 fraction of the deposited film. A transmission electron microscope (JEOL 2010F) with 200 kV acceleration voltage and Schottky emitter was used for the EELS investigations. The Schottky emitter together with an attached GATAN image filter allows the discrimination and quantification of the π^* and σ^* peaks of the carbon *K*-ionization edge in the EELS experiment.

An estimate of errors in the derived parameters is attempted through standard error propagation. An uncertainty in distances of 0.5 mm, and uncertainties estimated from shot-to-shot variation are propagated through to flow speeds, ion kinetic energies, forward peaking factors, and ion densities. In general, uncertainties in the plume parameters are found to be on the order of 10%.

III. RESULTS

A. Plume forward peaking parameter

Plume forward peaking parameters are calculated as discussed in the Experimental section. The amount of forward peaking is expected to increase with increasing spot size at constant laser energy density.[17,22] This effect is due to an increased number of collision events within the plume as spot size increases. The number of these oscillations is approximated as the ratio of the spot size to the mean free path. The adiabatic model[19] also predicts that an increase in the spot size will lead to a more forward peaked plume. This model gives an expression for the expansion of the plume in Cartesian geometry after the cessation of the laser pulse as

$$X(t)\frac{d^2X}{dt^2}=Y(t)\frac{d^2Y}{dt^2}=Z(t)\frac{d^2Z}{dt^2}=\frac{6kT_0(t)}{M}\left(\frac{X_0Y_0Z_0}{X(t)Y(t)Z(t)}\right)^{\gamma-1}. \quad (8)$$

In Eq. (7), *X*, *Y*, and *Z* represent the positions of the edge of the plume as functions of time; X_0, Y_0, and Z_0 represent the plume edge positions at the cessation of the laser pulse: *M* represents the mass of the particle in question; T_0 represents the plume temperature as a function of time, and gamma is the ratio of specific heats within the plume. At the time the laser pulse ceases, Eq. (8) reduces to

$$a_x=\frac{6kT_0}{X_0M}, \quad (9)$$

with similar expressions for the *Y* and *Z* coordinates. Let the *Y* and *Z* axes lie parallel to the target. The values of Z_0 and Y_0 are generally much larger than X_0. Examination of Eq. (9) shows that the initial acceleration will be greatest in the direction normal to the target. As spot size increases, the ratio of the acceleration of the plume normal to the target to that parallel to the target increases. Therefore, the plume expands in a forward peaked manner, the degree of which increases with spot size. In Fig. 4, the variation in forward peaking factor with increasing spot size is not discernable at low laser energy densities. At higher laser energy densities, the effect of spot size on forward peaking factor becomes noticeable.

Also shown in Fig. 4, there is an increase in the forward peaking parameter with an increase in laser energy density at constant spot size. At constant spot size, an increase in laser energy leads to increased particle density that in turn reduces the mean free path and, thereby, results in an increase in forward peaking factor.

B. Leading edge ion flow speeds and kinetic energies

Plume flow speeds are determined by comparing the arrival time of the leading edge of the plasma plume at the one and three centimeter Langmuir probe positions as discussed in the Experimental section. Figure 5 shows flow speeds as a function of laser energy density at different spot sizes. At constant spot size, the flow speed increases with increasing laser energy density. Ion flow results from pressure gradients present at the edge of the plume[17] leading to the conversion of thermal energy to expansion kinetic energy. It will be seen

Downloaded 11 Oct 2004 to 128.219.12.140. Redistribution subject to AIP license or copyright, see http://jap.aip.org/jap/copyright.jsp

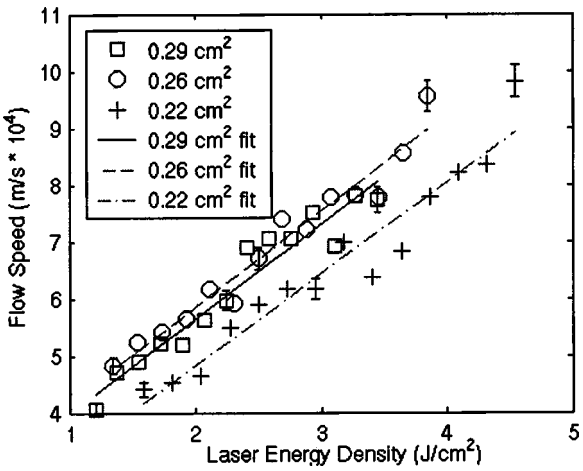

FIG. 5. Leading edge ion flow speeds as a function of laser energy density and spot size. Linear fit lines to the data are drawn to show trends.

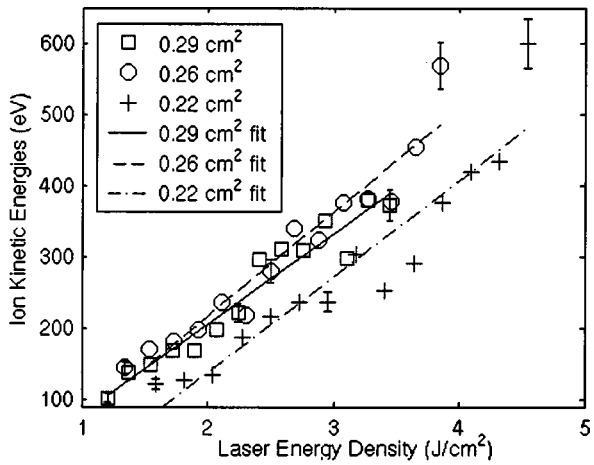

FIG. 6. Leading edge ion kinetic energies as a function of laser energy density. Linear fit lines to the data are drawn to show trends.

in the density results (Fig. 8) that increasing the laser energy density at constant spot size acts to increase the electron density. Increased densities measured at the Langmuir probe corresponds to increased densities at the target surface, and these higher densities correspond to higher density gradients at the plume edge. Therefore, higher flow speeds are expected when laser energy density is increased at constant spot size. Furthermore, increasing the laser energy density on the target at constant spot size represents an increase in the total amount of laser energy incident on the target, which increases the amount of energy available for conversion into kinetic energy through the adiabatic expansion process, as shown in Fig. 7, i.e., increased T_e with energy on target.

The dependence of flow speed on spot size at constant laser energy density is weak for the larger spot sizes. However, the flow speeds for the smallest spot size, 0.22 cm^2 are uniformly lower than the flow speeds at the larger spot sizes, 0.26 and 0.29 cm^2. This difference is due to the spot size effect on the adiabatic expansion of the plume. An increase in the spot size leads to an increase in the forward peaking of the plume. In the adiabatic model, when forward peaking is increased, the amount of energy converted from thermal energy to directed plume expansion kinetic energy increases. Furthermore, electron density increases with increasing spot size at constant laser energy density. As discussed previously, this increased electron density leads to increased pressure gradients at the plume edge, which leads to increased flow speeds.

Ion kinetic energies are shown as a function of laser energy density on the target are shown in Fig. 6. The range of ion kinetic energies is observed in this experiment to be 100 and 500 eV. These kinetic energies are larger than those cited previously[23] over a similar range of laser energy densities. However, spot size and hence total laser energy delivered to the target are larger in this work accounting for the differences seen. Recent work by Koivusaari *et al.*[12] shows a nearly identical range of ion kinetic energies, yet his energy densities are a factor of 10 higher.

C. Electron temperature

Electron temperature data are recorded at the different Langmuir probe positions, laser spot sizes, and laser energies. The dynamics of the plume can be investigated by examining the electron temperature at fixed Langmuir probe and lens positions. Figure 7 shows electron temperatures at the 1 cm Langmuir probe position versus laser energy density for different spot sizes. When laser energy density is held constant, the electron temperature decreases as the spot size increases. The effect of decreasing temperature with increasing spot size at constant laser energy density is a result of the forward peaking of the plume. More energy is converted from thermal energy to kinetic energy as spot size is increased. A consequence of the increased conversion of thermal energy to kinetic energy as spot size increases is that the plume is more forward directed. Electron temperature is then lower away from the target as spot size is increased.

Electron temperature also increases with increasing laser energy density at a constant spot size. The total amount of laser energy incident on the target is increased independent

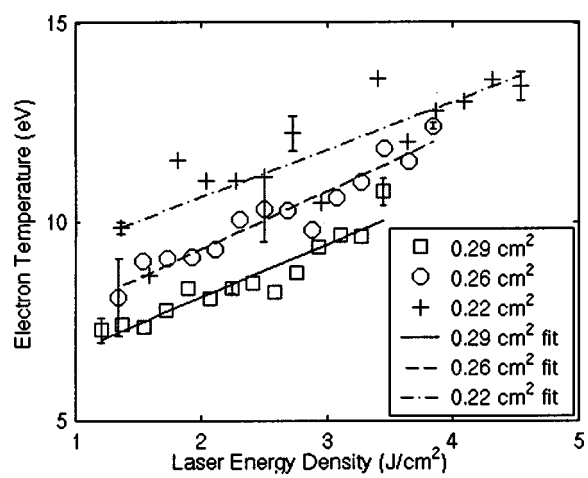

FIG. 7. Electron temperature at 1 cm. Langmuir probe position as a function of laser energy density and spot size. Linear fit lines to the data are drawn to show trends.

Downloaded 11 Oct 2004 to 128.219.12.140. Redistribution subject to AIP license or copyright, see http://jap.aip.org/jap/copyright.jsp

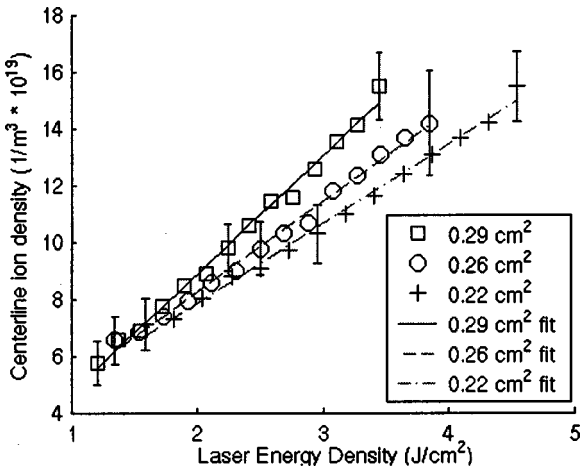

FIG. 8. Centerline ion densities at 1 cm Langmuir probe position as a function of laser energy density and spot size. Linear fit lines to the data are drawn to show trends.

of spot size, so more electron heating is possible. The absorption coefficient for the inverse bremsstrahlung process scales with the square of the ion density.[17] Increases in ion density will lead to an increasing amount of laser energy absorbed by the electrons. In this case, the increase in laser energy is more important than adiabatic expansion effects that convert thermal energy to kinetic energy due to increased forward peaking with laser energy density at constant spot size.

D. Ion densities

Ion densities at each Langmuir probe position are calculated from plume flow speeds and the electron temperatures employing Eq. (5). The centerline plume densities are then calculated from the local plume densities with the forward peaking values using Eq. (7). Figure 8 shows centerline plume densities as a function of laser energy density at the 1 cm Langmuir probe position for different spot sizes. If single ionization is assumed, the electron and ion densities are identical by charge neutrality. The increase in ion density with increasing laser energy density at constant spot size, and with increasing spot size at constant laser energy density, is explained in terms of collisional processes within the plasma plume.

The process of inverse bremsstrahlung heats electrons in the plasma plume. These heated electrons proceed to lose thermal energy by heating and ionizing neutral particles present in the plume. The amount of power absorbed in the inverse bremsstrahlung process can be expressed as

$$P_{\mathrm{IB}} = P_0(1 - e^{-\alpha_p X}) \tag{10}$$

where α_p is the inverse bremsstrahlung coefficient, x is the dimension of the plume, and P_0 is the power delivered. Increasing the total amount of delivered power will also increase the total amount of absorbed power, and therefore the temperature of the electrons increases. The rate at which ionization events occur is proportional to the electron-neutral collision frequency, which is proportional to the electron thermal speed. An increase in electron temperature will, therefore, cause an increase in the volumetric ionization rate. During the isothermal heating phase[19] neutral densities are near the solid density, therefore the electron-neutral collision rates are high, implying that energy transfer is rapid from the electrons to the neutral particles. Ionization acts to cool the electron fluid, while any excess energy from the ionization process heats the newly formed ions. The processes of electron heating by inverse bremsstrahlung and cooling by collisional ionization of the neutral particles compete for absorbed incident laser energy and result in a non-linear increase in electron temperature with increasing laser energy. Thus, charged particle density increases linearly with increasing laser energy density, even if the bulk electron temperature increases in a non-linear fashion.

The increase in ion density with increasing spot size at constant laser energy density is also consistent with the increase in plume forward peaking. The heavy particle density (including both neutrals and ions) spatial profile can be expressed as[9]

$$n(r,\theta) = \frac{m+1}{4\pi\Delta} N \frac{\cos^m \theta}{r^2}, \tag{11}$$

where m is the forward peaking factor, N is the total number of particles released per pulse, r is the radial distance from the target, θ is the polar angle from normal to the target surface, and Δ is the plume extent given as 0.05 m.[9] Thus, as the plume forward peaking increases, the heavy particle density is expected to increase along the centerline.

E. DLC thin film analysis

A 100 Å DLC film was deposited and prepared for electron energy-loss spectroscopy as described in the Experimental section. Figure 9 shows the K shell electron energy loss spectrum from the deposited 100 Å DLC thin film. The π^* and the σ^* antibonding peaks are readily visible. Following the method described by Kulik,[24] the sp^2/sp^3 fraction in this film is found by dividing the integral intensity of the π^* peak by the integral intensity of the π^* and σ^* antibonding peaks summed together. The result from this calculation is normalized to the identical comparison from a graphite reference material that is completely sp^2 bonded.[24,25] One minus this result is the sp^3/sp^2 fraction. The calculation is performed on the plot shown and results in the fraction of sp^3/sp^2 bonded carbon atoms in the thin DLC film to be 72.2%.

Confirmation that a high quality DLC film has been produced is derived from examination of the plasmon peak. The position of this low energy loss peak varies with the presence of diamond, DLC, or graphite.[24,25] Figure 10 shows the low energy plasmon loss peak for the deposited DLC film. The plasmon peak for diamond is at 33.8 eV, while the plasmon peak for this film is roughly 29 eV. The DLC plasmon peak cited in Ref. 25 occurs at 30.2 eV. Thus, we have created a high quality DLC film using our experimental conditions.

Downloaded 11 Oct 2004 to 128.219.12.140. Redistribution subject to AIP license or copyright, see http://jap.aip.org/jap/copyright.jsp

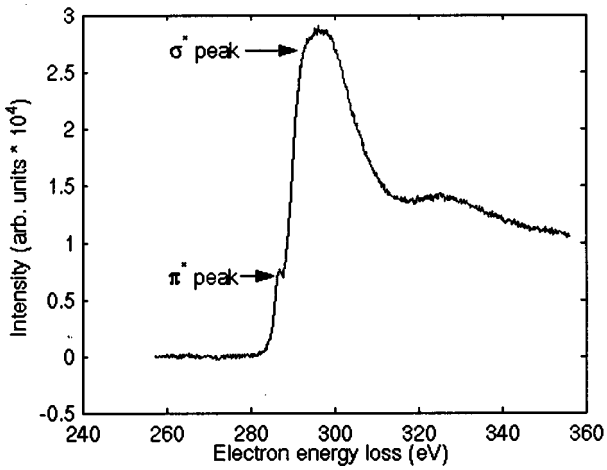

FIG. 9. Electron energy-loss spectrum for thin DLC film.

IV. CONCLUSIONS

Langmuir probe analysis on the plasma plume created during pulsed laser deposition of DLC was performed. Laser energy density on target, spot size, and Langmuir probe position were varied as independent variables. Ion flow speeds, ion kinetic energies, plume forward peaking values, and centerline densities were determined from raw temperature and density data. Finally, a high quality DLC film was deposited and found to have an sp^3/sp^2 bonding ratio of 72.2% with EELS in the TEM.

Plume forward peaking values (m) were determined using a logarithmic best-fit method. Peaking values were found to be between 8 and 15, indicating a highly forward peaked plume. The plume forward peaking value increased as a function of laser energy density and spot size. The cause of this effect is increased collisionality in the developing stages of the plume. The results are consistent with theoretical models describing forward peaking.

From raw density data, flow speeds were calculated. Flow speeds increased with laser energy density, due to increased density gradients and an increasing amount of energy transferred from thermal to kinetic energies. Leading edge ion kinetic energy is immediately calculated from flow speeds. These energies were found to be between 100 and 500 eV.

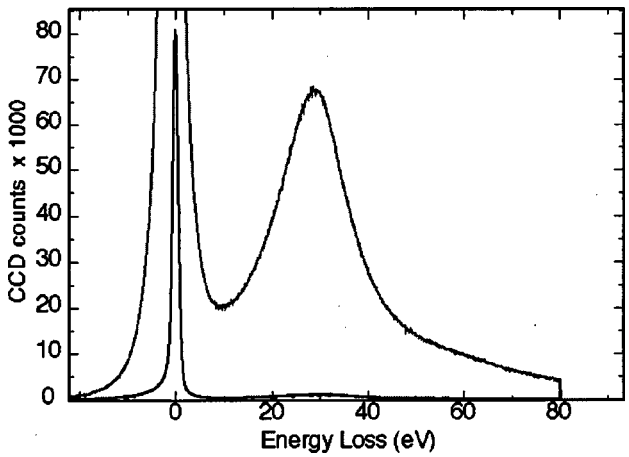

FIG. 10. Plasmon peak for thin DLC film from electron energy loss spectrum. The peak is magnified 10× to show detail.

Electron temperatures decreased with increasing spot size at constant laser energy density, and increased with increasing laser energy density at constant spot size. This, too, was found to be consistent with the adiabatic expansion model. Centerline densities of electrons are calculated from electron temperature, flow speed, and forward peaking value. Density increased both with spot size and laser energy density. An increasing electron-neutral collision rate was used to explain increases in electron density with laser energy density at constant spot size. Increase in electron density with increasing spot size at constant laser energy density is explained in terms of plume forward peaking.

Finally, a thin DLC film was deposited on Si(100). A chemical polishing technique devised by one of the authors was used to prepared the film for EELS avoiding ion implantation that introduces damage in the ion beam thinning process.[20] Using this technique, it is possible to determine sp^3/sp^2 bonding fraction without introducing the artifacts of ion beam thinning. It was determined through the electron energy loss spectroscopy technique that the deposited film was 72.2 percent sp^3/sp^2 bonded. Examination of the plasmon peak indicates that the deposited film is indeed a high quality DLC film.

ACKNOWLEDGMENTS

This work was conducted under the auspices of the National Science Foundation, Center for Advanced Materials and Smart Structures.

[1] Q. Wei and J. Narayan, Int. Mater. Rev. **45**, 133 (2000).
[2] J. Krishnaswamy, A. Rengan, J. Narayan, K. Vedan, and C. J. McHaurge, Appl. Phys. Lett. **54**, 2455 (1989).
[3] Q. Wei, R. J. Narayan, A. K. Sharma, J. Sankar, and J. Narayan, J. Vac. Sci. Technol. A **17**, 3406 (1999).
[4] R. J. Narayan, Q. Wei, A. K. Sharma, J. J. Cuomo, and J. Narayan, Mater. Res. Soc. Symp. Proc. **526**, 355 (1998).
[5] Q. Wei, A. K. Sharma, R. J. Narayan, N. M. Ravindra, S. Oktyabrsky, J. Sankar, and J. F. Muth, Mater. Res. Soc. Symp. Proc. **526**, 331 (1998).
[6] K. Lmimouni, C. Legrand, C. Dufour, A. Chapton, and C. Belouet, Appl. Phys. Lett. **78**, 2437 (2001).
[7] Q. Wei, J. Sankar, and J. Narayan, Surf. Coat. Technol. **146-147**, 250 (2001).
[8] D. H. Lowndes, V. I. Mekrulov, A. A. Puretzky, D. B. Geohegan, G. E. Jellison, Jr., C. M. Rouleau, and T. Thundat, Mater. Res. Soc. Symp. Proc. **526**, 325 (1998).
[9] R. M. Mayo, J. W. Newman, Y. Yamagata, A. Sharma, and J. Narayan, J. Appl. Phys. **86**, 2865 (1999).
[10] R. M. Mayo, J. W. Newman, Y. Yamagata, A. Sharma, and J. Narayan, J. Appl. Phys. **88**, 4154 (2000).
[11] J. Levoska and S. Leppavuori, Appl. Surf. Sci. **86**, 180 (1995).
[12] K. J. Koivusaari, J. Levoska, and S. Leppavuori, J. Appl. Phys. **85**, 2915 (1999).
[13] M. Chhowalla, A. C. Ferrari, J. Robertson, and G. A. J. Armaratunga, Appl. Phys. Lett. **76**, 1419 (2000).
[14] V. I. Merkulov, D. H. Lowndes, G. E. Jellison, Jr., A. A. Puretzky, and D. B. Geohegan, Appl. Phys. Lett. **73**, 2591 (1998).
[15] D. L. Pappas, K. L. Sanger, J. J. Cuomo, and R. W. Dreyfus, J. Appl. Phys. **72**, 3966 (1992).
[16] J. J. Cuomo, D. L. Pappas, J. Bruley, J. P. Doyle, and K. L. Sanger, J. Appl. Phys. **70**, 1706 (1991).
[17] D. H. Lowndes, in *Pulsed Laser Ablation and Desorption*, edited by J. C. Miller and R. F. Haglund (Academic, New York, 1998), Chap. 11.

Downloaded 11 Oct 2004 to 128.219.12.140. Redistribution subject to AIP license or copyright, see http://jap.aip.org/jap/copyright.jsp

[18] S. B. Segall and D. W. Koopman, Phys. Fluids **16**, 1149 (1973).
[19] R. K. Singh and J. Narayan, Phys. Rev. B **41**, 8843 (1990).
[20] J. Narayan and J. Fletcher, in *Defects in Semicondcutors*, Mater. Res. Soc. Symp. Proc. **2**, 191 (1981).
[21] R. K. Singh, D. Bhattacharya, and J. Narayan, Appl. Phys. Lett. **57**, 2022 (1990).
[22] K. L. Sanger, J. Appl. Phys. **70**, 5629 (1991).
[23] J. W. Newman, Jr., Master's thesis, North Carolina State University (1999).
[24] J. Kulik, Y. Lifshitz, G. D. Lempert, J. W. Rabalais, and D. Marton, J. Appl. Phys. **76**, 5063 (1994).
[25] S. D. Berger, D. R. McKenzie, and P. J. Martin, Philos. Mag. Lett. **57**, 285 (1988).

Downloaded 11 Oct 2004 to 128.219.12.140. Redistribution subject to AIP license or copyright, see http://jap.aip.org/jap/copyright.jsp